Energy Conversion and Management 342 (2025) 120125

Contents lists available at ScienceDirect

Energy Conversion and Management

journal homepage: www.elsevier.com/locate/enconman

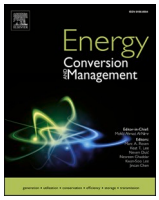

Metals and hydrogen derivatives for long-distance energy supply–A techno-economic comparison

Julia Schuler [a,*], Jannik Neumann [b], Armin Ardone [a], Frank Dammel [b], Peter Stephan [b], Wolf Fichtner [a]

[a] Institute for Industrial Production, Chair of Energy Economics, Karlsruhe Institute of Technology (KIT), Hertzstraße 16, 76187 Karlsruhe, Germany
[b] Institute for Technical Thermodynamics, Technical University of Darmstadt, Peter-Grünberg-Straße 10, 64287 Darmstadt, Germany

ARTICLE INFO

Keywords:
Power-to-X
Hydrogen
Metal Fuels
Synthetic Energy Carriers
Energy Supply Costs
Iron
Aluminum

ABSTRACT

Renewable energy carriers that are easy to transport and store are a key component of transnational energy trade in the global energy transition. This study compares six different energy carriers for long-distance energy supply; encompassing hydrogen, ammonia, methanol and synthetic methane, and, notably, metal fuels – specifically iron and aluminum. Drawing upon extensive techno-economic analyses spanning the entire energy supply chain, aluminum and iron emerge as particularly promising options for long-distance energy supply due to advantageous transport and storage properties combined with moderate conversion costs and the absence of costly intermediates such as carbon dioxide. The inclusion of comprehensive sensitivity analyses provides valuable insights into the suitability of these energy carriers for the transport and storage of renewable energy, further contributing to the understanding of their role in transforming the global energy landscape.

1. Introduction

Synthetic secondary energy carriers (ECs), which store renewable energy in chemical compounds, will play an important role in decarbonizing global energy systems, particularly for demand regions with constrained renewable electricity generation potentials, sectors with limited electrification feasibility, and long-term energy storage [1–3]. While hydrogen is an attractive option for pipeline-based energy trade, research indicates that for overseas energy supply, the significant costs for hydrogen liquefaction often make the production of derivatives such as ammonia, methanol, or synthetic methane – via the synthesis of hydrogen with nitrogen or carbon dioxide – more favorable [4–6].

Moreover, the potential of metals as renewable, zero-carbon ECs has drawn more attention in recent years from researchers worldwide [7–13]. Iron and aluminum are regarded as particularly promising metal ECs due to their abundance in the earth crust, their cyclability, and the implemented and scalable technologies for reducing their metal oxides [7,8,14–17]. Compared to hydrogen and hydrogen derivatives, iron and aluminum offer higher volumetric energy densities (see Table 1), simple storage and transport as solid bulk material, and feature no direct exports of water in the form of hydrogen molecules from the energy supply countries.

Research has primarily focused on material properties and technical aspects of the energetic use of metals, such as reaction kinetics, combustion mechanisms, energy cycle efficiency, cyclability, handling requirements, and infrastructure retrofit options [7–20].[1] However, to date, only a few studies have incorporated economic evaluations regarding the use of metal fuels: Ersoy et al. [24] present a techno-economic analysis on the use of aluminum as an energy carrier for simultaneous electricity and hydrogen production in a fuel station business case. Their findings indicate that aluminum is economically competitive when compared to a system that incorporates hydrogen cavern storage. Boudreau et al. [25] evaluate aluminum, liquid hydrogen and ammonia in a power-to-power system design for a remote mine, finding that the aluminum path can provide electricity at costs similar to those of the more commonly considered hydrogen derivatives. Neumann et al. [26] conduct a comparative analysis between iron and hydrogen for electricity generation in several case studies with different combinations of exporting and importing countries. The results indicate

* Corresponding author.
E-mail addresses: julia.schuler@kit.edu (J. Schuler), neumann@ttd.tu-darmstadt.de (J. Neumann), armin.ardone@kit.edu (A. Ardone), dammel@ttd.tu-darmstadt.de (F. Dammel), pstephan@ttd.tu-darmstadt.de (P. Stephan), wolf.fichtner@kit.edu (W. Fichtner).

[1] These investigations into metals as ECs have to be differentiated from the extensive research on metal hydride hydrogen storage [21–23]. In the context of metal hydrides, the metal functions solely as a medium for hydrogen storage and is not directly energetically used.

https://doi.org/10.1016/j.enconman.2025.120125
Received 14 February 2025; Received in revised form 2 June 2025; Accepted 25 June 2025
Available online 28 June 2025

Glossary

Symbols

CF	Capacity factor
COE	Cost of energy
COHE	Cost of hybrid electricity
COPH	Cost of process heat
CORE	Cost of renewable electricity
CRF	Capital recovery factor
d	Distance in km
e	Specific energy demand
ERC	Energy-related costs
ic	Specific investment costs
IRC	Investment-related costs
lt	Economic lifetime
ORC	Operation-related costs
TRC	Transport-related costs
tstore	Storage duration
z	Discount rate
ΔH_R	Heat of reaction
w	Specific material demand
γ	Operation cost factor
μ	Expected value
σ	Standard deviation

Subscripts/superscripts

const	Constant
EC	Energy carrier
el	Electricity
fluc	Fluctuating
HE	Hybrid electricity
heat	Process heat
H2buf	Hydrogen buffer
H2comp	Hydrogen compressor
k	Sub-process
Prod	Final product
RE	Renewable electricity
th	Thermal
tra	Transport

Abbreviations

Al	Aluminum
Al_2O_3	Alumina
ASU	Air separation unit
CEPCI	Chemical engineering plant cost index
CH_4	(Synthetic) Methane
CO_2	Carbon dioxide
CO	Carbon monoxide
DAC	Direct air capture
EC	Energy carrier
Fe	Iron
Fe_2O_3	Hematite
H_2	Hydrogen
H_2O	Water
MeOH	Methanol
N_2	Nitrogen
N_2O	Nitrous oxide
NH_3	Ammonia
NOx	Nitrogen oxides
PSC	Point source capture
PV	Photovoltaic

Table 1
Material properties of ECs [5,18,26].

Energy Carrier	Density [kg/m^3]	Lower heating value [kWh/kg]	Volumetric energy density [kWh/l]
Iron	7,870	2.05	9.68
Aluminum	2,700	8.60	14.10
Hydrogen (l)	71	33.33	2.37
Ammonia (l)	682	5.17	3.52
Methanol (l)	792	5.53	4.38
Methane (l)	450	13.50	6.08

comparable energetic efficiencies between the two options, but economic advantages for iron due to the retrofitting potential of existing infrastructure and superior transport and storage characteristics.

While numerous studies compare energy supply costs using hydrogen derivatives [6,27–29], a notable gap remains in the literature regarding comparative analyses that juxtapose multiple metal fuels and hydrogen derivatives as secondary ECs from an economic perspective. Addressing this identified research gap, this study conducts a comprehensive comparative evaluation of six promising secondary ECs for long-distance energy supply, iron (Fe), aluminum (Al), hydrogen (H_2), ammonia (NH_3), methanol (MeOH) and synthetic methane (CH_4). The corresponding energy supply chains are compared with respect to costs at an abstract import destination, incorporating detailed depiction of ship transport, conversion processes, production of precursors, and storage of intermediate and final products. A particular focus is placed on the impact of uncertainty, which is critical due to the involvement of many technologies at an early stage of development. Appendix A1 offers concise profiles of the examined six ECs.

2. Materials and methods

This section outlines the framework for evaluating the supply chains of the six ECs, including the set of equations employed, definitions of relevant terminology as well as materials and data used as input. Furthermore, a base case is defined and respective sensitivity studies are introduced.

2.1. Data collection

Data for the techno-economic analysis was gathered by a comprehensive analysis of recent literature. The analyses refer to the year 2030, parameters are chosen accordingly whenever possible. Given that many of the technologies under consideration currently have a low technology readiness level or are available only at pilot scale, sensitivity analyses are conducted to address uncertainties in, for example, investment costs, or energy demands.

The conversion of any parameter initially specified in terms of mass or volume to refer to energy content employs the density and gravimetric energy density of the respective EC, cf. Table 1. For the calculation of volumetric energy densities from the respective density and lower heating value, a void fraction of 0.4 was assumed for the two metals as powdery solids [30].

Restricting input parameters to be based on publications of the past ~ 5 years supersedes the need to convert costs to the same reference year. Costs are expressed in euros; for the conversion from US dollars to euros, the daily closing exchange rate averaged over the previous year of the respective year of publication is used, see Table 2.

Table 2
Exchange rates for the conversion from US dollars to euros.

Year	Yearly average of daily closing exchange rate [31]
2023	0.92415
2022	0.95113
2021	0.84572
2020	0.87700
2019	0.89329
2018	0.84745

2.2. System boundary and EC-specific process chains

Fig. 1 illustrates the scope for the evaluation of EC supply chains. The detailed assessment of each stage allows for the comprehensive comparison of cost of energy (COE_{EC}) at the importing site. The COE_{EC} are defined as specific cost relative to the energy content supplied to the importing site, calculated using the lower heating value (cf. Table 1).

Regarding electrical energy usage, the study distinguishes between two modes: processes can either be directly coupled to local renewable electricity generation to benefit from low electricity costs, necessitating flexible operation in response to the fluctuating electricity supply. This is represented through a simplified static model based on average annual full-load hours and cost of renewable electricity (*CORE*). Within this framework, only the electrolyzer and the compressor for 250 bar hydrogen buffer storage operate flexibly along renewable electricity supply. For the remaining electricity-dependent processes, higher-cost "hybrid electricity supply" (cost of hybrid electricity, *COHE*) is employed to support continuous operation.[2] These processes are executed continuously at their nominal load, with minimal downtime due to, e.g., maintenance. This requires the inclusion of buffer storage tanks for pressurized hydrogen to couple intermittent hydrogen production with subsequent baseload processes.

Besides respective synthesis (for hydrogen derivatives) or reduction (for metals) processes, relevant sub-processes are considered: direct air capture (DAC) and point source capture (PSC)[3] are implemented as two options for carbon dioxide (CO_2) supply to the methanol and methane synthesis; furthermore air separation units (ASU) for nitrogen (N_2) production, and liquefaction stages. The scope of the analysis further extends to cover storage and transportation of the (liquefied) ECs, providing a holistic view of the entire supply chain from the synthesis/reduction in an abstract exporting country to the provision of the ECs at a likewise unspecified import location. In the context of transportation, only long-distance international shipping is considered, without the inclusion of intermediate modes of transportation. As both start and end point of the supply chains remain abstract, the former only defined by local electricity costs and full-load hours and the latter by the transport distance from the exporting region, the variation of all three parameters in the sensitivity analysis allows to represent numerous potential combinations of energy partnerships. This analysis intentionally avoids specifying a use case for the imported energy, acknowledging the diverse options such as electricity generation, high-temperature heat supply, and transportation, notably aviation and shipping, all of which are being explored both in the context of hydrogen derivatives and metal fuels [3,20,25,32].

Costs associated with water supply to the electrolysis are not considered, predicated on the understanding that the impact from the inclusion of seawater desalination on the overall costs of hydrogen production is negligible. Incorporating reverse osmosis, the current leading desalination technology, is estimated to increase the energy demand by no more than 0.2 % and add approximately $0.01 per kilogram of hydrogen to production costs [33].

For both iron and aluminum, feedstock costs for the metal powders are omitted based on the assumption that the particles can undergo an unlimited number of consecutive reduction and oxidation cycles, making them, in principle, a permanent asset [8]. Neumann et al. demonstrate that feedstock costs are negligible for the iron cycle, even with a small number of cycles [26]. This assumption is extended to aluminum, as its feedstock costs (approximately 0.3 € per kilogram alumina, which translates to ~ 0.6 € per kilogram of aluminum, given that 1.9 kg of alumina are required to produce one kilogram of aluminum [24,34]) are of a similar order of magnitude relative to its energy content: 0.6 €/kg_{Al} / 8.6 kWh/kg_{Al} = 70 €/MWh_{Al}, compared to iron with feedstock costs of ~ 0.23 €/kg_{Fe} [26] and an energy content of 2.05 kWh/kg_{Fe}, resulting in 112 €/MWh_{Fe}. When allocating the initial investment in the powders to the energy content, even with a conservative usage period of 20 years, four oxidation–reduction cycles per year, and a discount rate of 3 %, the costs are reduced to 1.2 €/MWh_{Al} and 1.9 €/MWh_{Fe}, respectively, which is negligible (~1 %) compared to the energy supply costs observed in our results.

2.3. Energy supply chain modeling

The calculation of COE_{EC} at the import site for each respective EC includes investment-related costs (*IRC*), operation-related costs (*ORC*) covering both operation and maintenance, and energy-related costs (*ERC*) for all process steps k (ASU, DAC, PSC, electrolysis, reduction, synthesis, liquefaction and storage) along the EC-specific process chain (cf. Fig. 1), as well as transnational maritime transport costs (*TRC*). Costs are considered pre-tax and constant over the project's entire economic lifespan.

$$COE_{EC} = IRC_{EC} + ORC_{EC} + ERC_{EC} + TRC_{EC} \left[\frac{€}{\mathrm{MWh_{EC}}}\right] \quad (1)$$

ERC comprise costs for intermittent renewable electricity supply (*CORE*), for constant hybrid electricity supply (*COHE*), and for process heat (*COPH*), paired with respective energy demands (e_k) for all process steps k:

$$ERC_{EC} = \sum_k \left(e_{RE,k}CORE + e_{HE,k}COHE + e_{heat,k}COPH\right) \left[\frac{€}{\mathrm{MWh_{EC}}}\right] \quad (2)$$

IRC are determined from the specific investment costs (ic_k) and the capacity factor (CF_k) (i.e., CF_{fluc} for fluctuating processes and CF_{const} for variable processes) by applying the capital recovery factor (*CRF*), which is based on the economic lifetime lt_k and the discount rate z.

$$IRC_{EC} = \sum_k CRF_k \cdot \frac{ic_k}{CF_k \cdot 8760\mathrm{h}} = \sum_k \frac{(1+z)^{lt_k} \cdot z}{(1+z)^{lt_k} - 1} \cdot \frac{ic_k}{CF_k \cdot 8760\mathrm{h}} \left[\frac{€}{\mathrm{MWh_{EC}}}\right] \quad (3)$$

ORC are frequently given as a share γ_k of the specific investment costs:

$$ORC_{EC} = \sum_k \gamma_k \cdot \frac{ic_k}{CF_k \cdot 8760\mathrm{h}} \left[\frac{€}{\mathrm{MWh_{EC}}}\right] \quad (4)$$

The calculation of *IRC*, *ORC* and *ERC* for final product storage requires an additional information: the total storage duration of the final product before shipping $tstore_{Prod}$ in days. *IRC* and *ORC* for storage units are multiplied by $tstore_{Prod} \cdot (365 days)^{-1}$.

[2] The term "hybrid" lacks explicit definition concerning whether it denotes renewable generation and supplementary grid purchase or involves the incorporation of battery storage. While our base scenario assumes renewable electricity generation paired with utility-scale battery storage in (see section 2.4), the sensitivity analyses consider a broader range of COHE, which may also reflect renewable electricity generation complemented by grid electricity supply (see section 2.5). However, in such cases of grid-supported electricity supply, it cannot be guaranteed that the produced ECs are fully carbon neutral.

[3] Recycling CO_2 from point sources into synthetic ECs is not a carbon–neutral concept, as fossil carbon is ultimately released into the atmosphere during combustion. However, it offers an interesting and, in terms of economics and technology readiness, a more realistic benchmark case for 2030.

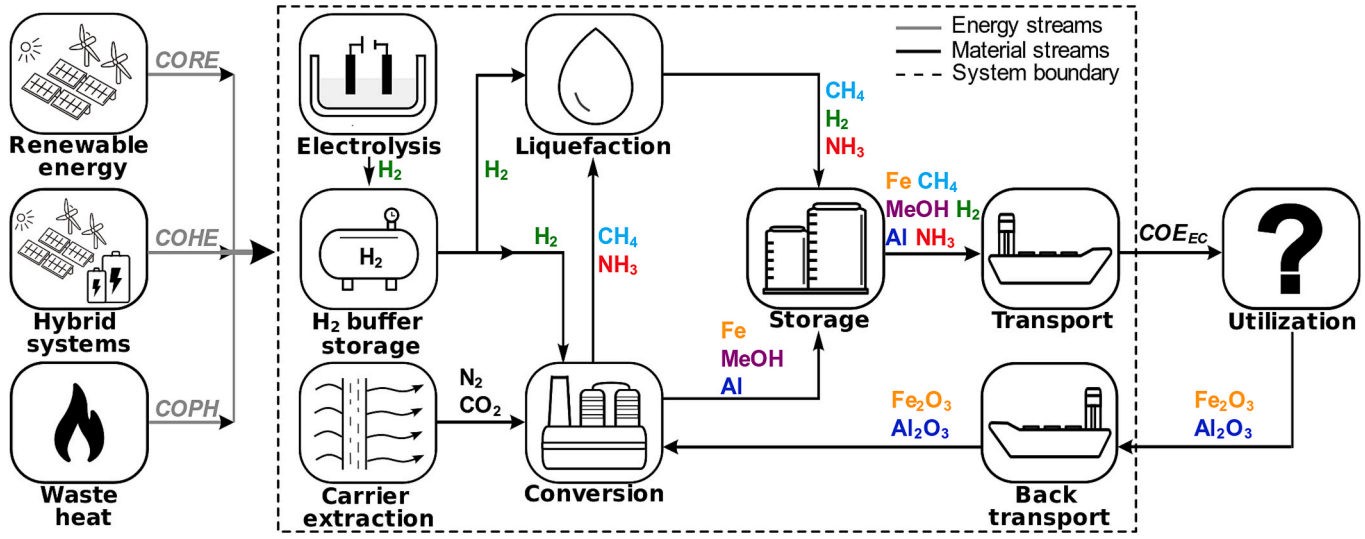

Fig. 1. Energy supply chains with corresponding material streams.

A pressurized hydrogen buffer storage system is included to balance fluctuating hydrogen supply from electrolysis with subsequent continuous liquefaction, synthesis or iron reduction processes. The size and costs of the required pressurized hydrogen tank are based on the intermediate hydrogen storage duration $tstore_{H_2buf}$, w_{EC,H_2} represents the specific hydrogen demand for the synthesis/reduction of the EC, and ic_{H_2buf} the specific costs for the pressurized hydrogen tank.

$$IRC_{EC,H_2buf} = CRF_{H_2buf} \cdot \frac{tstore_{H_2buf}}{365\text{days}} w_{EC,H_2} \cdot ic_{H_2buf} \left[\frac{€}{\text{MWh}_{EC}}\right] \quad (5)$$

IRC are calculated separately for the compressor of the 250 bar hydrogen buffer storage:

$$IRC_{EC,H_2comp} = CRF_{H_2comp} \cdot \frac{ic_{H2comp}}{CF_{fluc} \cdot 8760\text{h}} w_{EC,H_2} \left[\frac{€}{\text{MWh}_{EC}}\right] \quad (6)$$

In the assessment of maritime transport-related costs TRC_{EC}, specific costs e_{tra} per energy content and distance are utilized and multiplied with the transport distance d_{tra} and a multiplier for the return journey ($1 + \delta_{EC}$). Given that these ships typically return empty from the importing site back to the exporting site, $\delta_{EC} = 1$ is set for hydrogen and derivatives. Ships would presumably not carry any additional products on their return journeys, as these vessels are highly specialized. Instead, empty ships often take on ballast water to ensure proper maneuverability [35]. However, for the metallic ECs, the oxidized (depleted) EC must be returned to the exporting site. Due to the binding of oxygen to the metals, the increase in mass to be transported is considered ($\delta_{Fe} = 1.43, \delta_{Al} = 1.89$).

$$TRC_{EC} = d_{tra}(1 + \delta_{EC}) e_{tra,EC} \left[\frac{€}{\text{MWh}_{EC}}\right] \quad (7)$$

2.4. Base scenario data

Table 3 presents a set of general parameters applicable to all ECs, most of which are subject in the sensitivity analyses. A real discount rate of 3 % is employed. Renewable electricity costs *CORE* of 40 €/MWh represent average photovoltaic (PV) and favorable onshore wind electricity generation sites projected for the year 2030 [36]. Hybrid electricity costs *COHE* are set at 100 €/MWh, in accordance with the findings from Schmidt et al. [37] for 2030 utility-scale lithium-ion battery storage and Lazard [38] for PV-battery or wind-battery hybrid systems.

Process heat is relevant for three processes: DAC and PSC, which operate at temperatures below 150 °C for the regeneration step using amine solvent materials, the most mature technology [39,40]; and iron oxide reduction, which occurs at approximately 800 °C in the shaft furnace [41,42]. Heat pumps are assumed to supply heat for both carbon capture processes, as discussed in the literature for DAC [29,43–45] and PSC [40,46,47]. Using a coefficient of performance of 2.5 and hybrid electricity costs, *COPH* of 40 €/MWh are determined for DAC and PSC. For the reduction of iron oxide, higher-temperature process heat is assumed to be provided by electric resistance heaters, as seen in many current studies on hydrogen-based iron ore reduction [41,42,48]. Assuming 100 % efficiency for these heaters, *COPH* are equivalent to the costs of hybrid electricity supply *COHE* at 100 €/MWh for iron reduction. The capacity factor *CF* is linked to the electricity supply mode, as operation aligned with dynamic electricity supply (full load hours following [36]) results in reduced utilization while hybrid supply enables baseload operation. The total storage duration of the final product $tstore_{Prod}$ before shipping is set at 14 days as in [28], meanwhile the hydrogen buffer storage should cover three days of non-production of the electrolyzer [49]. A shipping distance d_{tra} of 15,000 km in the base scenario could exemplify, e.g., trade between Europe and Southern Africa or Southern America.

Table 3
General input parameters for the base scenario.

Parameter		Value
Discount rate	z	3 %
Renewable electricity costs	*CORE*	40 €/MWh
Hybrid electricity costs	*COHE*	100 €/MWh
Process heat costs iron reduction	*COPH*	100 €/MWh
Process heat costs DAC and PSC	*COPH*	40 €/MWh
Capacity factor fluctuating processes	CF_{fluc}	37.5 %
Capacity factor baseload processes	CF_{const}	90 %
Final product storage duration	$tstore_{Prod}$	14 days
Hydrogen buffer storage duration	$tstore_{H_2buf}$	3 days
Transport distance	d_{tra}	15,000 km

Table 4 lists the input parameter values attributed to conversion (electrolysis, DAC, PSC, air separation, synthesis, reduction, liquefaction) and storage processes in the base scenario, whenever possible representing the reference year 2030. All specifications for material demands adhere to stoichiometric reactions. The specifications for the electrolyzer incorporate anticipated advancements in proton exchange membrane (PEM) technology expected by 2030, characterized by its flexibility in operation. Parameters for aluminum smelting reflect the Hall-Héroult process with inert anodes, as full commercialization is

Table 4
Summary of key techno-economic parameters for storage and conversion processes.

Process	Specific energy demand e_k		Specific investment costs ic_k		Specific operation costs γ_k		Lifetime lt_k		Specific material demand w_{EC}/ boil-off	
Water electrolysis	52.90 kWh_{el}/kg_{H2}	[56]	650 €/kW_{el}	[56]	4 %/a	[56]	20 a	[56]	–	[56]
H_2 liquefaction	6.78 kWh_{el}/kg_{H2}	[29]	1,498 €/kW_{H2}	[29]	8 %/a	[29]	20 a	[29]	–	
H_2 liquid storage	*Boil-off reliq.*		26 $/$kg_{H2}$	[56]	2 %/a	[56]	20 a	[56]	Boil off: 0.1 %/d	[56]
H_2 buf. storage – tank	–		450 €/kg_{H2}	[43]	2 %/a	[43]	20 a	[43]	–	
H_2 buf. storage – compr.	1.71 kWh_{el}/kg_{H2}	[43]	88 €/kW_{H2}	[43]	4 %/a	[43]	15 a	[43]	–	
Fe reduction	0.75 kWh_{el}/kg_{Fe} 0.41 kWh_{th}/kg_{Fe}	[41]	414 €/(t_{Fe}/a)	[57]	12.4 €/t_{Fe}/a	[57]	40 a	[57]	54.1 kg_{H2}/t_{Fe}	
Fe/Al storage (silos)	–		446 $/$m^3$	[52]	2 %/a		40 a		–	
Alumina smelting	10.64 kWh_{el}/kg_{Al}	[51]	3,880 $/($t_{Al}$/a)	[51]	56 €/t_{Al}/a	[51]	20 a	[51]	–	
Air separation	0.25 kWh_{el}/kg_{N2}	[29]	10,942 €/GW_{el}	[29]	4 %/a	[29]	20 a	[29]	–	
Haber-Bosch synthesis	1.5 kWh_{el}/kg_{NH3}	[6]	714 $/$kW_{NH3}$	[6]	4 %/a	[6]	25 a	[6]	0.18 kg_{H2}/kg_{NH3} 0.82 kg_{N2}/kg_{NH3}	
NH_3 storage	–		0.9 €/kg_{NH3}	[58]	5 %/a	[58]	30 a	[58]	–	
Direct air capture	0.32 kWh_{el}/kg_{CO2} 2.00 kWh_{th}/kg_{CO2}	[43]	6,624 €/(kg_{CO2}/h)	[43]	4.95 %/a	[59]	25 a	[59]	–	
Point source capture	0.03 kWh_{el}/kg_{CO2} 0.85 kWh_{th}/kg_{CO2}	[59]	2,500 €/(kg_{CO2}/h)	[59]	3 %/a	[59]	25 a	[59]	–	
MeOH synthesis	0.1 kWh_{el}/kg_{MeOH}	[60]	1,090 €/kW_{MeOH}	[60]	30 €/kW_{MeOH}/a	[60]	30 a	[60]	0.2 kg_{H2}/kg_{MeOH} 1.37 kg_{CO2}/kg_{MeOH}	
MeOH storage	–		42 €/MWh_{MeOH}	[43]	2 %/a	[28]	30 a	[28]	–	
CH_4 synthesis	0.18 kWh_{el}/kg_{CH4}	[3]	735 $/$kW_{CH4}$	[3]	4 %/a	[3]	30 a	[3]	0.5 kg_{H2}/kg_{CH4} 2.74 kg_{CO2}/kg_{CH4}	
CH_4 liquefaction	0.5 kWh_{el}/kg_{CH4}	[29]	740 €/kW_{CH4}	[29]	3.5 %/a	[29]	25 a	[29]	–	
CH_4 storage	*Boil-off reliq.*		611.59 €/m^3	[29]	2 %/a	[29]	20 a	[29]	Boil-off: 0.076 %/d	[61]

expected by 2030 [50,51]. Energy demands for the re-liquefaction of methane and hydrogen storage boil-offs are assumed to be equivalent to the initial liquefaction process, while the liquefaction of ammonia is integrated into the synthesis process. While heat demands are included for DAC, PSC and iron reduction, it is assumed that the pre-heating requirements of certain exothermic synthesis processes (e.g., Haber-Bosch) are met through internal heat recovery within the respective process. For iron reduction, techno-economic parameters are adopted from the shaft furnace direct reduction with hydrogen, including subsequent fusing in an electric arc furnace to facilitate atomization of lump iron to fine iron powders (cf. Appendix A1). It is anticipated that alternative reduction processes would be implemented if iron is to be utilized as an EC. These advanced routes are promising as they could circumvent the energy-intensive fusing step by maintaining particle size, potentially lowering energy and capital costs significantly. However, at present, techno-economic parameters are not sufficiently published. Carbon steel silos are assumed for storage of aluminum and iron to prevent unwanted re-oxidation. The investment costs are determined based on [52] and updated using a recent (2024) chemical engineering plant cost index (CEPCI).

Specific shipping costs in the year 2030 for hydrogen, ammonia, methanol and methane are taken from a recent review article [53]. For iron and aluminum, assuming a stable landscape in bulk shipping without significant developments that would lead to notable changes in associated costs, transport costs are calculated using a 15,000 €/day time charter rate for a dry bulker with 64,000 tons capacity [54]. Bulk cargoes are carried in multiple sealed cargo holds. An average ship speed of 24 km/h is assumed (13 knots) [55]. Considering the increase in mass for the return journey of the oxidized metals ($\delta_{Fe} = 1.43, \delta_{Al} = 1.89$), shipping costs of 0.05 €/(GWh · km) and 0.2 €/(GWh · km) are projected for aluminum and iron, respectively.

2.5. Sensitivity analyses

Two different forms of sensitivity analysis are conducted to identify key sub-processes and parameters. First, the sensitivity of energy supply costs to variations in individual input parameters is examined through local sensitivity analysis. Additionally, Monte Carlo simulations are implemented to investigate sensitivity towards variations in multiple input parameters simultaneously by randomly generating values for these input parameters from pre-defined probability distributions. The probability distributions for each examined input parameter are presented in Table 5. Uniform distributions are employed for location-specific parameters. For instance, in the context of various energy export locations, there exists a range of possible electricity costs and transport distances, and no particular value is deemed "more plausible" than another. Renewable electricity costs *CORE* and full load hours, represented by the capacity factor CF_{fluc}, span a range from excellent PV to average wind electricity generation sites [36]. Hybrid electricity costs *COHE* reflect the range of electricity supply costs from hybrid battery storage systems [37,38], as well as backup grid power supply in potential energy-exporting countries [28], and determine heat costs *COPH* as described above. Transport distances d_{tra} cover the entire spectrum of economic EC shipping along global trade routes [5]. Ranges for storage durations and baseload process capacity factors are selected in discretion of the authors.

On the other hand, process-specific electricity and heat demands and

Table 5
Probability distribution of examined input parameters in the Monte Carlo analyses. Categorization in n**ormal (N) or uniform (U) distribution.**

Input parameter			Range
Renewable electricity costs	*CORE*	U	20–60 €/MWh_{el}
Hybrid electricity costs	*COHE*	U	60–180 €/MWh_{el}
Capacity factor fluct. processes	CF_{fluc}	U	20–55 %
Capacity factor baseload processes	CF_{const}	U	85–95 %
Final product storage duration	$tstore_{Prod}$	U	2–30 days
Hydrogen buffer storage duration	$tstore_{H2buf}$	U	1–5 days
Transport distance	d_{tra}	U	5.000–25.000 km
Specific investment costs	ic_k	N	μ = base case,
Low uncertainty			σ = 10 % of base case
High uncertainty			σ = 50 % of base case
Specific electricity demands	$e_{el,k}$	N	μ = base case,
Specific heat demands	$e_{heat,k}$	N	σ = 10 % of base case
Ship transport costs	*TRC*	N	μ = base case,
Low uncertainty			σ = 10 % of base case
High uncertainty			σ = 50 % of base case

investment costs for electrolysis, ASU, DAC, PSC, reduction, syntheses, liquefaction and storage plants, as well as ship transport costs, are modeled as normal distributions.[4] The expected value μ of the distributions is aligned with the base scenario value, representing an approximate average obtained from thorough analyses of recent literature. The standard deviation σ is selected as 10 % of it for all energy demands. Given that a normal distribution has 95.4 % of values falling within the interval of +/- two σ from μ, this choice allows for the analysis of input parameters within a range of +/-20 % around base scenario values, a range consistent with the majority of literature values. However, for investment costs, we distinguish between processes with higher and lower uncertainty in the development of plant investment costs until 2030. Higher investment cost uncertainty is modeled with a σ of 50 % for electrolysis, DAC, iron reduction (due to the potential for implementing alternative methods, such as flash iron making or fluidized bed processes), alumina reduction (owing to the low technology readiness of inert anode technology), hydrogen liquefaction, and liquid hydrogen storage. A lower σ of 10 % is assigned to the 2030 investment costs of more established processes, namely ASU, PSC, ammonia synthesis, methanol synthesis, methane synthesis, methane liquefaction, and the storages for iron, aluminum, pressurized hydrogen, ammonia, methanol, and liquid methane.

Similarly, we model ship transport of liquid hydrogen with a σ of 50 % due to its low technology readiness, whereas transport of all other ECs is assigned a σ of 10 %, as these can draw on established maritime transport chains [53].

Parameters are assumed to be independent within the Monte Carlo simulations, however, in reality, interrelations may exist (e.g., availability and costs of fluctuating electricity).

3. Results and discussion

First, the composition of energy supply costs for the ECs in the base scenario are analyzed. To enhance the understanding of the systems behavior under varying conditions, findings from detailed sensitivity analyses are presented. Local sensitivity analyses are first undertaken to identify critical parameters within each energy supply chain. Through this approach, the impact of individual variables on the system's performance is quantitatively assessed. Furthermore, comprehensive global sensitivity analyses are conducted to explore the responsiveness of the system to simultaneous variations in several input parameters, thereby identifying a distribution of supply costs for the different ECs.

Fig. 2 shows the results of the supply cost analysis for all six investigated ECs in the base scenario. The energy supply costs for the importing country in the year 2030 range from 162 €/MWh for aluminum to 206 €/MWh for methane with CO_2 from DAC. The iron energy supply chain results in 179 €/MWh, methane with PSC in 178 €/MWh, and methanol in 170 €/MWh and 204 €/MWh with PSC and DAC, respectively. Hydrogen and ammonia both exhibit costs of 188 €/MWh.

In terms of the composition of total costs, aluminum stands out as 98.7 % of costs are related to the reduction/smelting step. The Hall-Héroult process is powered by electricity and doesn't require any intermediate products. Also, due to the easy handling as a solid bulk material, storage and shipping costs are negligible.

Storage costs of the final product are minor for all ECs for the considered storage duration of 14 days, with the highest costs observed for liquid hydrogen storage at 2.4 €/MWh or 1.3 % of total supply costs. Transport costs are more significant, comprising 13.0 % of total supply costs for hydrogen, and between 1.3 % and 4.9 % for the other ECs. The comparatively high cost projections for hydrogen storage and transportation are primarily related to the exceptionally low boiling point at −253 °C and the current lack of utility scale infrastructures. The same factors explain why liquefaction accounts for a significant 25.8 % of hydrogen supply costs.

For all ECs except aluminum, hydrogen production dominates supply costs, constituting a share between 47.7 and 69.1 %. Intermediate pressurized hydrogen storage contributes significantly to total costs with a share between 7.4 and 10.7 %. Compared to nitrogen costs for ammonia synthesis (9.9 €/MWh) and PSC for methanol and methane (16.0 €/MWh and 13.1 €/MWh, respectively), costs associated with DAC are understandably much higher with 50.0 €/MWh for methanol and 41.0 €/MWh for methane due to the lower concentration of carbon dioxide in air, as well as the limited technology readiness of DAC, whereas air separation and PSC are well-established processes. Appendix A2 presents a breakdown of the base scenario's energy supply costs into investment-related (*IRC*), operation-related (*ORC*), energy-related (*ERC*), and transport costs (*TRC*).

To validate our model, it is essential to compare its cost projections with those reported in the existing literature. However, this is challenging for aluminum and iron, as publications that examine the use of metal fuels from an economic perspective are sparse. In the 2024 vision document of *Metalot*, a network organization dedicated to the research in metal fuels, energy supply costs of iron are compared with those of hydrogen and its derivatives. Notably, their cost projections for iron are comparatively low at 120 €/MWh, but they fall within their cost range of ammonia and methanol [62]. The energy supply costs for aluminum reported by Boudreau et al. are slightly higher than those in our base case, primarily due to the choice of a higher specific electricity consumption for the Hall-Héroult process [25].

However, a validation of our model results for hydrogen and its derivatives is possible due to an extensive and active research landscape with numerous recent publications. To validate our results against current literature, three country cases – Australia, Namibia and the US – are investigated. Four key parameters are modified in these country cases based on recently published country-specific data for 2030. These parameters are *CORE*, derived from the 2030 PV electricity generation costs presented by Kleinschmitt et al. [36] (Fig. 3, page 12) as well as transport distances to Germany, discount rate and *COHE* based on Moritz et al. [6], as shown in Table 6. While the original source provides wholesale electricity price projections in $/MWh, we adopted the same values in €/MWh for our calculations, as projecting future exchange rates introduces significant uncertainties. Since the study by Moritz et al. [6], against which we compare our supply costs, models DAC-based CO_2 supply for methanol and methane production, we have only included these scenarios in our model validation, excluding those involving PSC.

Comparing the results from our country cases shown in Fig. 3 with those of Moritz et al. for supply costs in 2030 (Fig. 6 in their publication), we observe that our results align well with their ranges for hydrogen (120–180 €/MWh), ammonia (150–180 €/MWh), methanol (160–210 €/MWh) and methane (160–200 €/MWh). Another recent study by Hank et al. on supply costs of hydrogen-based ECs for the year 2030 also examines Australia and Namibia as production countries with imports to Germany for hydrogen, ammonia and methanol [28]. They report significantly higher supply costs compared to Moritz et al., ranging from 217 to 270 €/MWh for liquid hydrogen, 173–213 €/MWh for ammonia and 192–240 €/MWh for methanol (Fig. 6-3 in their publication). This highlights the substantial uncertainty surrounding future costs of supply chains for renewable synthetic ECs.

A local sensitivity analysis is conducted to assess the sensitivity of supply costs to individual input parameters. The parameters selected for this analysis include those listed in Table 3 (note that heat supply costs depend on electricity supply costs, as described in Section 2.4), as well as energy demands and investment costs from Table 4. Operational costs and the lifetime of process equipment were excluded for conciseness,

[4] We exclude the PSC-based production of methanol and methane from the global sensitivity analyses in Fig. 5, as the resulting histograms with eight data series become overly complex, compromising legibility. However, we added the corresponding results for PSC-based methanol and methane production in Appendix A3.

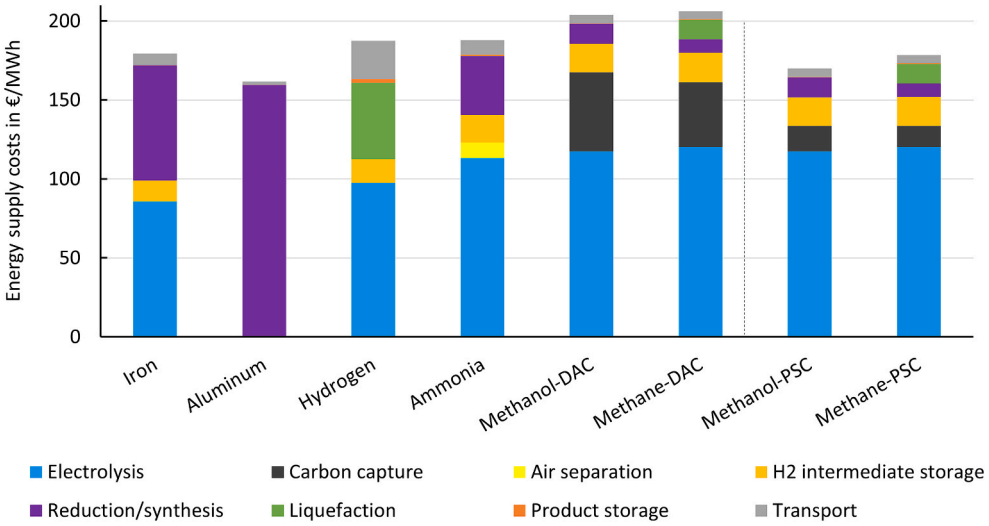

Fig. 2. Components of energy supply costs for all investigated ECs.

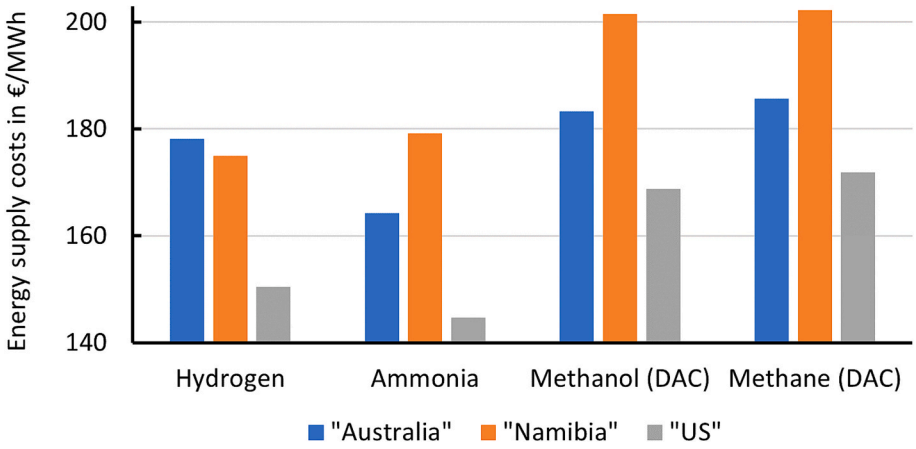

Fig. 3. Results from the country cases used for model validation.

Table 6
Input parameters modified in the country cases, based on [6,36].

	CORE[€/MWh$_{el}$]	**Distance** [km]	**Discount rate** [%]	***COHE***[€/MWh$_{el}$]
"Australia"	25	21,000	6	64
"Namibia"	17	10,720	8	144
"US"	25	8,320	6	28

given their minor impact on supply costs.

While keeping all other parameters constant, single parameters are varied by + 20 % from the base scenario values, except for the capacity factors, which are decreased by 20 %. The results shown in Fig. 4 mark the influence of each parameter variation on energy supply costs.

The findings underline the critical role of electricity costs for the economic attractiveness of all ECs, as a combined 20 % increase in both fluctuating (*CORE*) and constant electricity supply costs (*COHE*) results in an energy supply cost increase greater than 9 % for all ECs. For all non-metallic ECs, an increase in *CORE* has a greater impact than an increase in *COHE*, as baseload synthesis, liquefaction and precursor production processes consume significantly less energy compared to intermittent hydrogen production. In contrast, the supply chains of iron and aluminum involve baseload processes with substantial electricity demands, making them more sensitive to increased *COHE*.

The analysis further highlights the crucial role of future developments in electrolyzer technology. For all ECs (except aluminum, which does not include hydrogen production in its supply chain), a 20 % increase in the electrolyzer's specific electricity demand has a substantially greater impact on supply costs than increased electricity or heat demands in the respective reduction, synthesis or liquefaction plants, or the DAC/PSC/ASU processes. A 20 % rise in electricity demand of the electrolyzer has a slightly smaller effect to a 20 % increase in *CORE*, as fluctuating electricity does not only power the electrolyzer, but also the hydrogen compressors. Also in terms of sensitivity to investment costs, the electrolyzer plays a more prominent role compared to other plants. Only the sensitivities of investment costs for hydrogen liquefaction and the alumina smelter show comparable effects on supply costs.

The local sensitivity analysis reveals that aluminum is sensitive to fewer parameters, but the sensitivity to these parameters is considerably stronger compared to the other ECs.

To investigate sensitivity to variations in multiple input parameters simultaneously, Monte Carlo simulations are executed. These simulations generate a spectrum of possible supply costs for the ECs illustrated in Fig. 5, based on uncertainty ranges as specified in Table 5.

The upper histogram includes only the normal distributions for transport costs, electricity and heat demands, and specific investment costs for all processes (electrolysis, ASU, DAC, reductions, syntheses, liquefaction and storage). Consequently, the expected value (μ) corresponds to the deterministic base scenario solutions (cf. Fig. 2). In the lower histogram, in addition to the normal distributions, uniform

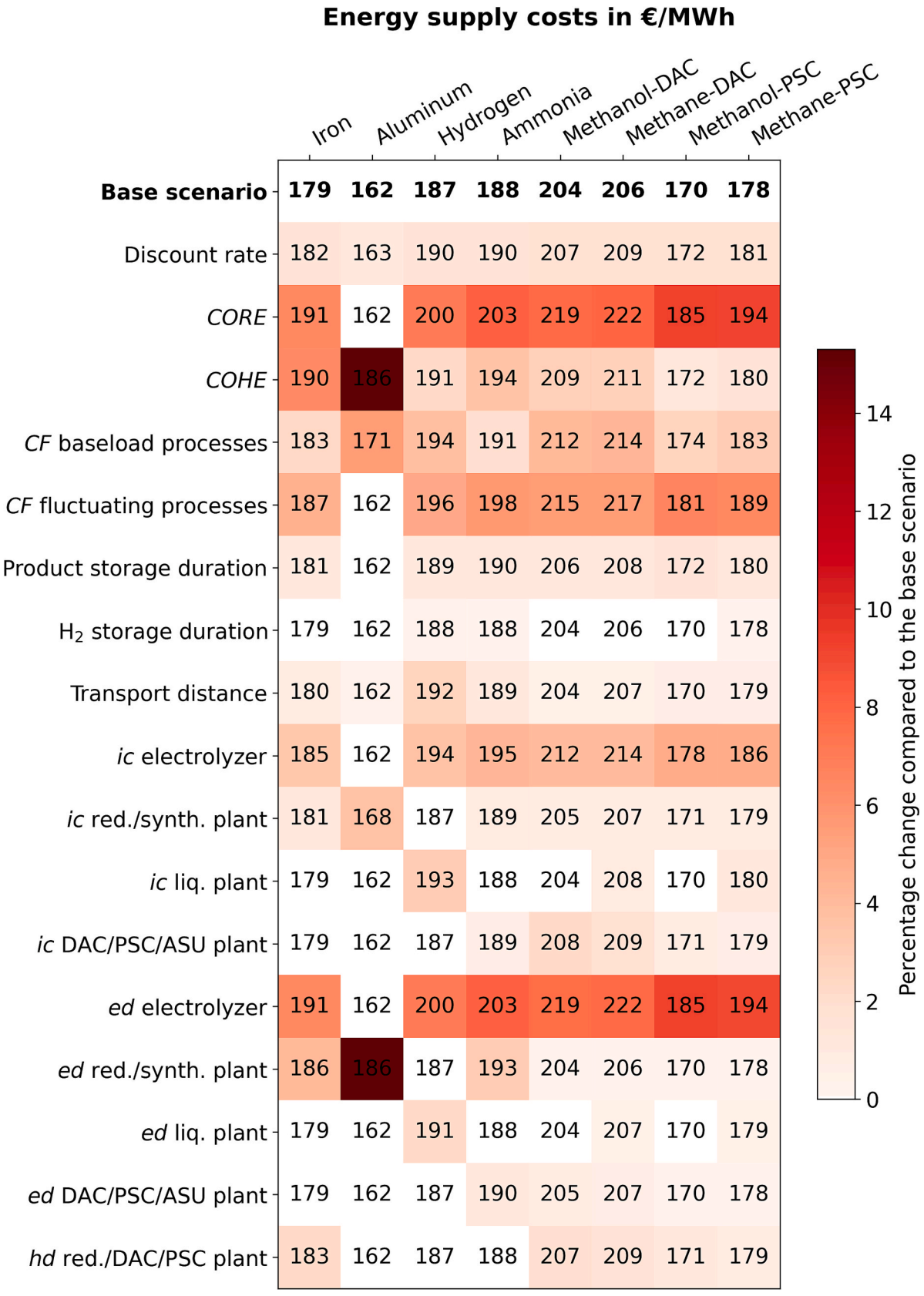

Fig. 4. Results from the local sensitivity analysis. Investigated is the impact of a 20 % increase in each respective parameter, except for the capacity factors (CF), which are decreased by 20 %. Abbreviations: *ic*: investment costs, *ed*: electricity demand, *hd*: heat demand; red.: reduction, synth. Synthesis, liq.: Liquefaction.

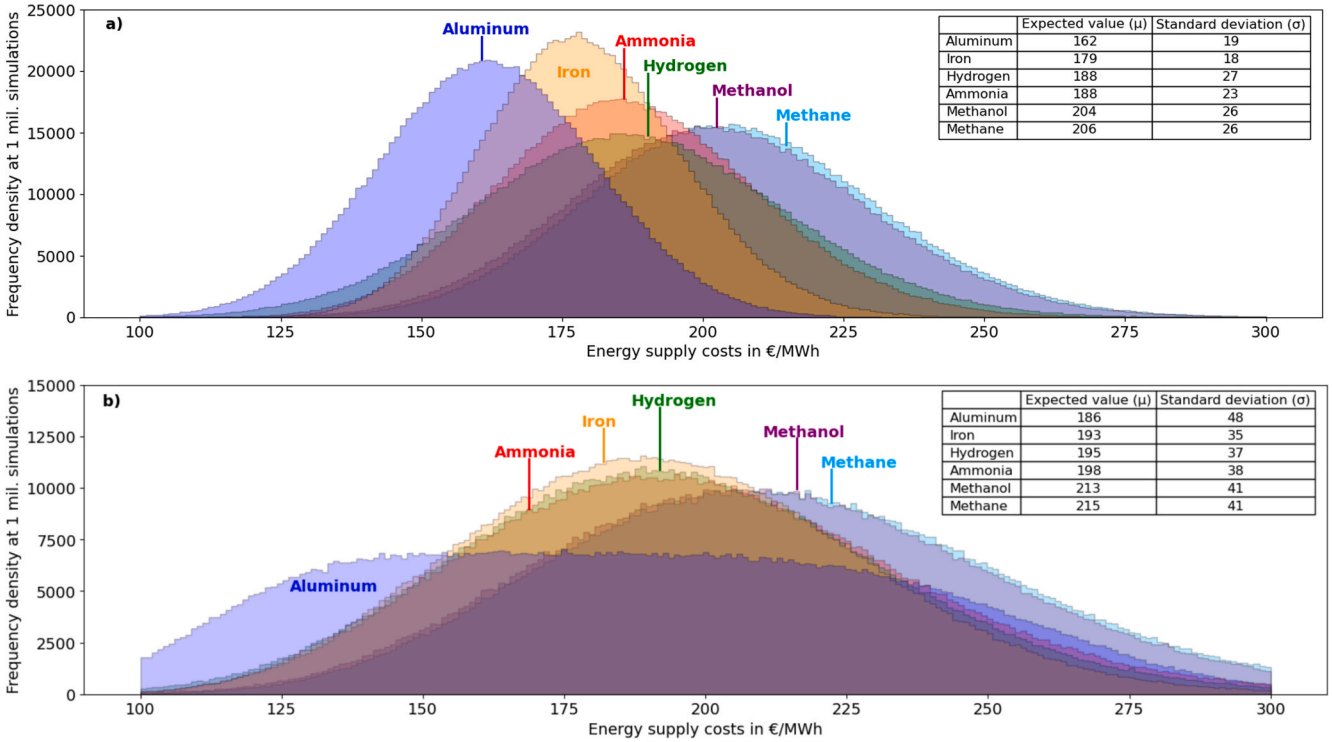

	Expected value (μ)	Standard deviation (σ)
Aluminum	162	19
Iron	179	18
Hydrogen	188	27
Ammonia	188	23
Methanol	204	26
Methane	206	26

	Expected value (μ)	Standard deviation (σ)
Aluminum	186	48
Iron	193	35
Hydrogen	195	37
Ammonia	198	38
Methanol	213	41
Methane	215	41

Fig. 5. Sensitivities to variations in a) energy demands and specific investment costs and b) additional process parameters.

distributions are applied for cross-process parameters (*CORE*, *COHE*, d_{tra}, $tstor_{Prod}$, $tstor_{H2buf}$, CF_{const}, CF_{fluc}) with individual parameter ranges, cf. Table 5. Total energy supply costs to the importing country are on the x-axis, divided into 200 equally sized intervals between 100 and 300 €/MWh. The y-axis is interpretable as the frequency (or probability) of cost values per interval, with the constant width of the intervals as proportionality factor. The total number of simulations amounts to one million for both the scenario yielding the upper and the lower histogram. While Fig. 5 presents DAC-based methanol and methane production, the results for PSC-based production are provided in Appendix A3, Fig. 7, to improve histogram readability.

In the upper histogram, where only process-specific techno-economic parameters are varied with a fixed relative uncertainty, the cost distribution curves for iron and aluminum cluster at the lower end of the spectrum, indicating both lower average supply costs and smaller uncertainty bands. This resilience arises because their supply chains depend on fewer capital-intensive steps: aluminum hinges almost entirely on the smelting process, while iron requires only hydrogen-based direct reduction and electrolysis. In contrast, the hydrogen, ammonia, methanol, and methane pathways involve several additional stages (e.g., air separation, cryogenic liquefaction, DAC), each of which introduces further uncertainty – consistent with the findings of the local sensitivity analysis (cf. Fig. 4). The narrower supply cost distributions for iron and aluminum imply more predictable supply costs, which, from an economic perspective, could be advantageous for long-term strategic planning and investment decisions.

However, the superiority of the metals weakens in the lower histogram, which additionally incorporates uniform distributions for cross-process, location-specific parameters like the costs of electricity supply, transport distances, and storage durations as specified in Table 5. The distribution of supply costs is wider for all ECs, and expected values experience an increase as the means of the applied uniform distributions are higher for certain parameters than the values from the base case, which were utilized in Fig. 5 a). Both the expected values μ and the standard deviations σ of iron and aluminum converge to those of the other ECs. While iron maintains a comparatively low expected value and standard deviation of supply costs, reaffirming its attractiveness under the conditions of this study, aluminum exhibits the most significant spread in its cost distribution, standing out as the only EC without a clear peak. The uniform distribution set for hybrid electricity costs *COHE* overlays the cumulative effects from the normal distributions set for investment costs and energy demands. The significant dependence on electricity costs for aluminum is also apparent in the local sensitivity analysis (cf. Fig. 4), as well as in Fig. 6 in Appendix A2, which shows that for aluminum, energy-related costs account for a much higher share – 76 % of total supply costs – compared to the other ECs. This highlights the substantial dependence of aluminum's economic competitiveness on the availability of cheap electricity.

It is important to point out that, due to the underlying methodology, the peaks of the distributions in Fig. 5 do not inherently signify the most probable costs for importing ECs in the future. Location-specific attributes, such as costs for electricity or heat and transport distances, are specific base scenario values in Fig. 5 a) and uniform distributions in Fig. 5 b), but without an indication of the anticipated volumes of EC production at an export site. Hence, the peaks reflect probabilities related to specific investment costs, electricity and heat demands of future processes, which are modeled in the input parameter set as normal distributions. However, the analysis ranks the degree of uncertainty associated with each respective energy carrier, providing decision-makers with insights to select supply chains that are both cost-effective and predictable.

4. Limitations and future work

It is important to recognize the limitations inherent to this assessment. The reliability of the results depends on the accuracy of the input parameters and the underlying assumptions, including the distributions used in the Monte Carlo simulations. To enhance the robustness of these results, further research is needed to refine data on processes that are in many cases not available on larger scale yet (e.g., Hall-Héroult process with inert anodes, hydrogen-based iron reduction, methane synthesis, DAC, liquid hydrogen shipping and storage).

The parameters for iron reduction are based on the shaft furnace direct reduction process using hydrogen which is being developed in the steel industry. This is followed by iron powder production through fusing in an electric arc furnace and atomizing the melt into fine iron powders. The atomization step is neglected in this analysis due to its negligible energy demand, approximately 1 % of the iron reduction process [63]. The shaft furnace reduction concept was chosen due to the lack of techno-economic data on innovative reduction processes, such as fluidized bed reactors or flash ironmaking, which are investigated for using iron powder as a fuel [30,63]. These processes are promising as the particle size remains constant during reduction, eliminating the need for melting in an electric arc furnace for atomization. This reduces capital and energy requirements and has the potential to further improve the competitiveness of iron.

Also, uncertainties arise with regard to the handling of ECs between supply chain steps, which could result in additional costs, e.g., measures to prevent the re-oxidation of metals or the boil-off of hydrogen and methane. Such efforts will bolster accuracy, fortifying the strategic insights derived from this analysis to provide guidance for energy policy and investment decisions towards sustainable and economically viable solutions.

The analyses refer to the year 2030 and do not allow for conclusions to be drawn for later time horizons, when relative economic attractiveness could change as, e.g., specific investment costs or energy demands for respective processes evolve differently.

An inclusion of energy usage can also impact the attractiveness of individual ECs. The versatility of ECs with regard to potential applications, coupled with divergent efficiencies in the conversion of final energy to end-use applications and opportunities for infrastructure re-use, holds the potential to improve the evaluation of ECs with higher energy supply costs. For instance, incorporating use cases could enhance the appeal of methane due to its compatibility with existing infrastructure and applications.

Subsequent research endeavors could also explore particular combinations of energy export and import sites, considering factors such as local renewable energy potential, the location-specific cost of capital, and transport infrastructures. While our model addresses the interplay between the time-dependent availability of energy supply and subsequent continuous processes by incorporating storages, the absence of a temporal dimension in modeling energy supply chains neglects further time-dependent effects, including storage fill levels, infrastructure occupancy and expansion, discontinuous ship traffic, and dynamic port operations.

The aforementioned aspects – consideration of EC utilization, specification of energy importers, exporters and trade routes, and temporal resolution – can be addressed by energy system modeling, which our presented analysis lays the foundation for. Comprehensive, spatially and temporally resolved global-scale energy system models enable the assessment of the potential role of each EC within an integrated energy system. By considering various complex interdependencies, these models facilitate the determination of an optimal technology mix for the global energy transition.

5. Conclusion

Global trade of synthetic ECs will play an important role in future energy systems. In this context, this study presents an economic analysis of hydrogen and its derivatives ammonia, methane, and methanol, as well as, for the first time, the two metals iron and aluminum, as secondary ECs for long-distance transport of renewable energy. A detailed techno-economic analysis of each EC and its corresponding energy supply chain is presented, including upstream processes (air separation and direct air capture), reduction and synthesis, and downstream processes (liquefaction, storage, maritime transport). The ECs are compared based on the costs of energy supply to an importing location, with 2030 as the reference year. The deterministic assessments for a base scenario are complemented by detailed local sensitivity analyses to identify crucial sub-processes and parameters, as well as Monte Carlo simulations to reveal the variability and risk profiles associated with each EC.

Aluminum and iron score well in the context of transportation and storage due to their inherent properties as solids. Aluminum emerges as the option with the lowest energy supply costs across a wide range of parameter settings; however, it also demonstrates an outstanding dependency on electricity costs. Iron demonstrates supply costs competitive with hydrogen and derivatives, and a low sensitivity to variations in key parameters. The wider supply cost distributions of aluminum could imply a riskier profile for aluminum as compared to iron; however, such a spread also indicates great potential for cost reduction if the influencing factors (e.g., electricity demand of the Hall-Héroult process) are managed effectively. In our analysis, ammonia and hydrogen exhibit supply costs comparable to those of iron, whereas methanol and methane imply higher costs. The supply costs for liquid hydrogen, methanol, methane, and ammonia were cross-validated with current literature. The findings from the sensitivity analyses also underscore the critical role of advancements in electrolyzer technology and the availability of cheap renewable electricity in enhancing the attractiveness of synthetic ECs.

In conclusion, this study provides a comprehensive comparison of energy carriers for long-distance energy supply, emphasizing the viability of the metal fuels iron and aluminum compared to hydrogen and hydrogen derivatives.

Declaration of Generative AI and AI-assisted technologies in the writing process

During the preparation of this work, the authors used DeepL and ChatGPT in order to improve readability and language. After using these tools, the authors reviewed and edited the content as needed and take full responsibility for the content of the published article.

CRediT authorship contribution statement

Julia Schuler: Writing – review & editing, Writing – original draft, Visualization, Validation, Software, Methodology, Investigation, Formal analysis, Data curation, Conceptualization. **Jannik Neumann:** Writing – review & editing, Writing – original draft, Visualization, Validation, Methodology, Formal analysis, Data curation, Conceptualization. **Armin Ardone:** Writing – review & editing, Supervision, Methodology. **Frank Dammel:** Writing – review & editing, Supervision, Methodology. **Peter Stephan:** Writing – review & editing, Supervision, Resources, Project administration, Funding acquisition. **Wolf Fichtner:** Writing – review & editing, Supervision, Resources, Project administration, Funding acquisition.

Funding

Funding by the Hessian Ministry of Higher Education, Research, Science and the Arts as well as the Strategy Fund of the KIT Presidium is gratefully acknowledged.

Declaration of competing interest

The authors declare that they have no known competing financial interests or personal relationships that could have appeared to influence the work reported in this paper.

Acknowledgments

This work was performed within the cluster project *Clean Circles*.

Appendix A1

Short profiles of ECs.

Aluminum (Al). The global production of primary aluminum reached 69 Mt in 2022 [64] while international trade of unwrought aluminum and aluminum alloys amounted to 28 Mt in 2021 [65]. The predominant method for converting alumina (Al_2O_3) into aluminum metal is the Hall-Héroult process with a global average specific energy consumption of 14.1 kWh/kg_{Al} in 2022 [66]. This process involves the electrolysis of a heated, molten alumina mixture at temperatures near 1,000 °C. A central component of this process, the carbon anodes, are consumed during the electrolysis in the Hall-Héroult cell [67]. A noteworthy advancement is the ongoing development of inert anode technology, which is approaching commercialization stage. This technological breakthrough promises substantial reductions in greenhouse gas emissions and energy savings [25,50], and it will reach a key milestone with a ten-pot, 100 kA demonstration plant at Rio Tinto's Arvida smelter in Québec, where first production is targeted for 2027 [68]. Progress is further illustrated by RUSAL's successful start-up of the first full-size inert-anode cell in November 2024 [69], lending confidence to expectations of wider market penetration from the late-2020 s into the early 2030 s [51].

To use aluminum as a zero-carbon fuel, energy can be released by combustion with air [34,70] or in a water oxidation mode [34,71], the latter yielding both heat and hydrogen.

Upon exposure to air, aluminum reacts immediately with oxygen, forming a protective aluminum oxide layer approximately two nanometers thick [72]. This thin oxide layer acts as a barrier, preventing further oxidation of the underlying metal [72], thereby facilitating the safe transport and storage of aluminum.

Ammonia (NH_3). Ammonia is a widely produced (150 Mt in 2022 [64]) and globally traded chemical (17.4 Mt in 2022 [73]). The production process involves reacting hydrogen with nitrogen (N_2) in the exogenous Haber Bosch synthesis [74] at elevated pressures (120–220 bar) and temperatures (400–450 °C):

$$N_2 + 3H_2 \rightarrow 2\,NH_3 \quad \Delta H_R = -92.44\,kJ\,mole^{-1} \tag{A.1}$$

While ammonia is predominantly produced from fossil fuels today, the production can be decarbonized by utilizing renewable energy for all subprocesses (i.e., hydrogen production, air separation, auxiliary energy) [74]. Beyond its current industrial use, mainly as a feedstock in fertilizer production [73], extensive experience and existing regulatory frameworks for its synthesis, transport, and usage have increased interest in ammonia as a secondary EC. Ammonia is a toxic and corrosive gas, but a substantial benefit, relative to methane and hydrogen, lies in its lower energy demands for liquefaction, owing to a much higher boiling point at –33 °C. Direct combustion of ammonia results in significant NO_x emissions, two orders of magnitude greater than natural gas combustion [75]. However, ongoing research and the development of advanced combustion systems have the potential in substantially reducing these emissions [75]. Additionally, the release of nitrous oxide (N_2O), a greenhouse gas and contributor to ozone layer depletion, determines whether green ammonia combustion can be considered climate friendly [76]. Alternatively, ammonia may undergo a cracking process to recover hydrogen and nitrogen; however, this entails considerable additional costs [58].

Hydrogen (H_2). The utilization of hydrogen as a zero-carbon energy carrier is considered fundamental in driving the energy transition due to its versatility and ease of production, as reflected by corporate and political strategies worldwide [77,78]. In 2022, global hydrogen production reached 95 Mt, primarily sourced from fossil fuels by steam reforming and coal gasification [79] for non-energetic use in fertilizer production and refining. Water electrolysis accounted for only 0.1 % of total hydrogen production [79]. However, a large number of electrolysis projects have been announced with the aim to produce in sum over 28 Mt of hydrogen by 2030 [79].

An inherent limitation of hydrogen is its low energy density per unit volume. For transportation over short to medium distances, the use of new or repurposed pipelines is the means of choice [80]. For longer distances, liquefying hydrogen or converting it to derivatives for maritime transport emerges as a more economically favorable option [80]. For the liquefaction step, existing commercial processes exhibit a specific energy consumption (SEC) that spans from 11.9 to 15 kWh per kg of hydrogen which translates into 35–45 % of the energy content and liquefaction costs of 2.5–3 $ per kg [81] owing to the very low boiling point at −253 °C. Specific liquefaction costs of around 1–2 $ per kg and energy requirements of 6–8 kWh per kg of hydrogen are anticipated for the near future with rising capacities [81]. However, large-scale liquid hydrogen (LH_2) vessels have not yet been realized. Their storage tanks would need to be approximately two orders of magnitude larger than the biggest existing LH_2 tanks. Globally, only a few utility-scale LH_2 storage facilities exist, the largest operational tank having a capacity of 3,200 m^3 and a 4,700 m^3 tank under construction, both managed by NASA [82]. The first and only LH_2 vessel in service is the Suiso Frontier, a diesel-powered pilot ship with a cargo capacity of 1,250 m^3 [83]. Large-scale liquid hydrogen shipping is considered feasible, but there are widely varying presumptions of prospective shipping costs [53].

Iron (Fe). The exploration of iron as an EC has gathered increasing interest, particularly following the pioneering research by Bergthorson et al. [7,14,84]. Its attractiveness lies in the feasibility of a carbon-free circular energy economy: energy is released by the oxidation of fine iron powders, producing heat that can be used in high-temperature applications or converted into electricity in retrofitted coal-fired power plants [20]. The emerging iron oxides can then be captured and recycled using renewable energy. The following Eq. (A.2) represents the thermochemical reduction reaction between (renewable) hydrogen and iron oxide (hematite, Fe_2O_3) as the energy storage step:

$$Fe_2O_3 + 3H_2 \rightarrow 2Fe + 3H_2O \quad \Delta H_R = 98.77\,kJ\,mole^{-1} \tag{A.2}$$

An advantage lies in the synergies with the iron and steel industry. Firstly, given a global iron ore production of 2,600 Mt in 2022 [64], production capacities are available on vast scale, rendering the production of additional iron for use as an EC non-critical [19]. Secondly, the iron and steel industry accounts for 7–9 % of global greenhouse gas emissions [85] and hence is also investigating hydrogen-based direct reduction processes for decarbonization [67,86]. For the steel industry, shaft furnace concepts are the most promising in the near future mainly due to maturity of the technology [87]. However, with regard to the specific requirements of using iron as an EC, there is a strategic advantage, both energetically and economically, in opting for reduction and oxidation processes that are compatible in terms of particle sizes. Implementing fluidized bed or flash ironmaking for the reduction step avoids additional process steps to adjust particle sizes. However, it is important to note that these approaches are still in the research phase.

Methanol (MeOH). Methanol, a flammable alcohol, is liquid at ambient conditions. With an approximate global annual production of around 80 Mt

it serves as a feedstock for the synthesis of many chemicals and is also in use as a fuel or fuel blending. It is mainly produced by hydrogenation of natural gas-based carbon monoxide at high pressures (50–100 bar) and 200–300 °C:

$$CO + 2H_2 \rightarrow CH_3OH \quad \Delta H_R = -91.8\text{kJ mole}^{-1} \tag{A.3}$$

The production of renewable methanol includes water electrolysis and carbon capture, followed by endothermic reverse water–gas shift reaction to convert carbon dioxide into carbon monoxide:

$$CO_2 + H_2 \rightarrow CO + H_2O \quad \Delta H_R = +41.2\text{kJ mole}^{-1} \tag{A.4}$$

The carbon dioxide for methanol synthesis can be captured from point sources (PSC) such as fossil fuel power plants or cement factories, or via direct air capture (DAC), involving large fans drawing ambient air over a chemical sorbent, either liquid or solid, and subsequent heating to separate the CO_2. Pricing DAC is challenging due to its early stage, with current costs ranging between $264 and $1,000 per ton of CO_2 [88]. Experts anticipate that future DAC costs might decrease to levels below $200 per ton of CO_2 [88].

Possible applications encompass the direct use of renewable methanol in internal combustion engines (with growing interest from the shipping industry), as well as in fuel cells or turbines [43]. Noteworthy advantages include the potential re-use of mineral oil infrastructures and the absence of sulfur oxides (SO_x), particulate matter (PM), and comparatively low nitrogen oxides (NO_x) emissions during combustion.

Synthetic Methane (CH_4). The existence of vast infrastructure and applications for natural gas offers a streamlined transition to using synthetic methane produced from renewable energy. The methanation, or Sabatier process, involves reacting carbon dioxide with hydrogen to produce methane and water at 1–5 bar and 300–450 °C:

$$CO_2 + 4H_2O \rightarrow CH_4 + 2\,H_2O \quad \Delta H_R = -164.9\text{kJ mole}^{-1} \tag{A.5}$$

Preceding the methanation, the production of renewable methane involves water electrolysis and carbon capture as described for methanol.

Appendix A2

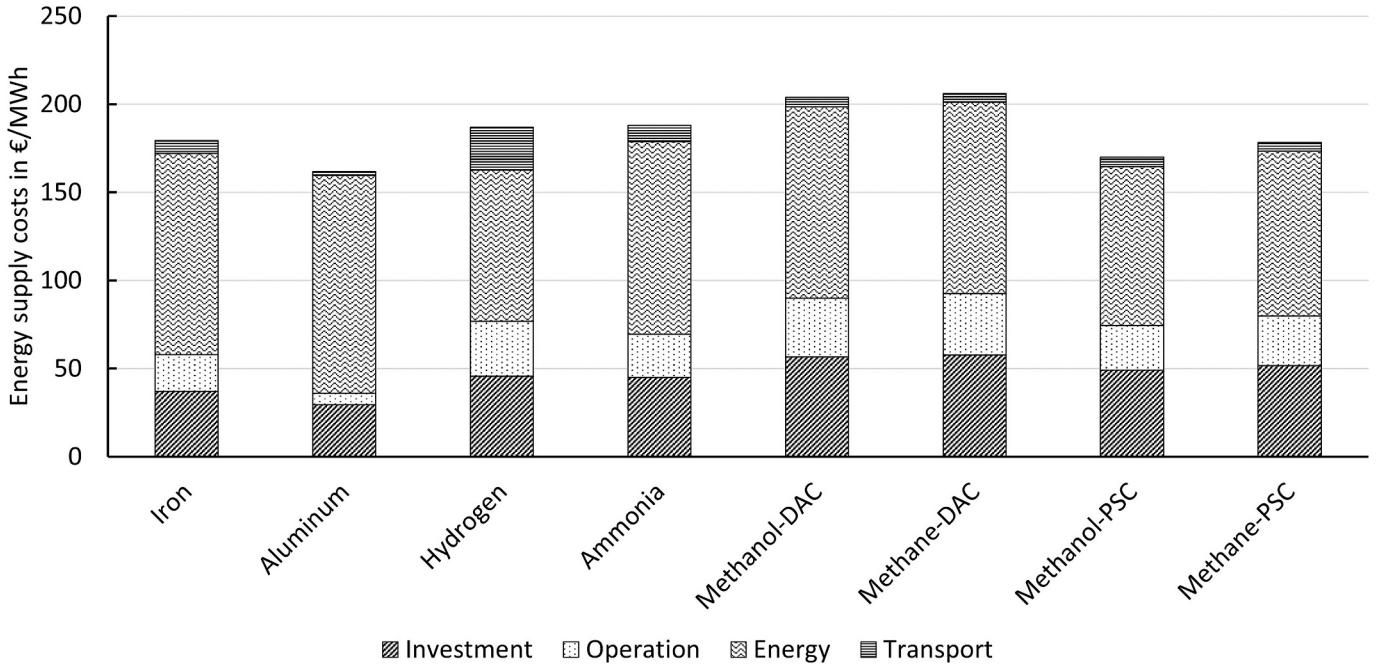

Fig. 6. Breakdown of the base scenario's energy supply costs into investment-related (IRC), operation-related (ORC), energy-related (ERC), and transport costs (TRC).

Appendix A3

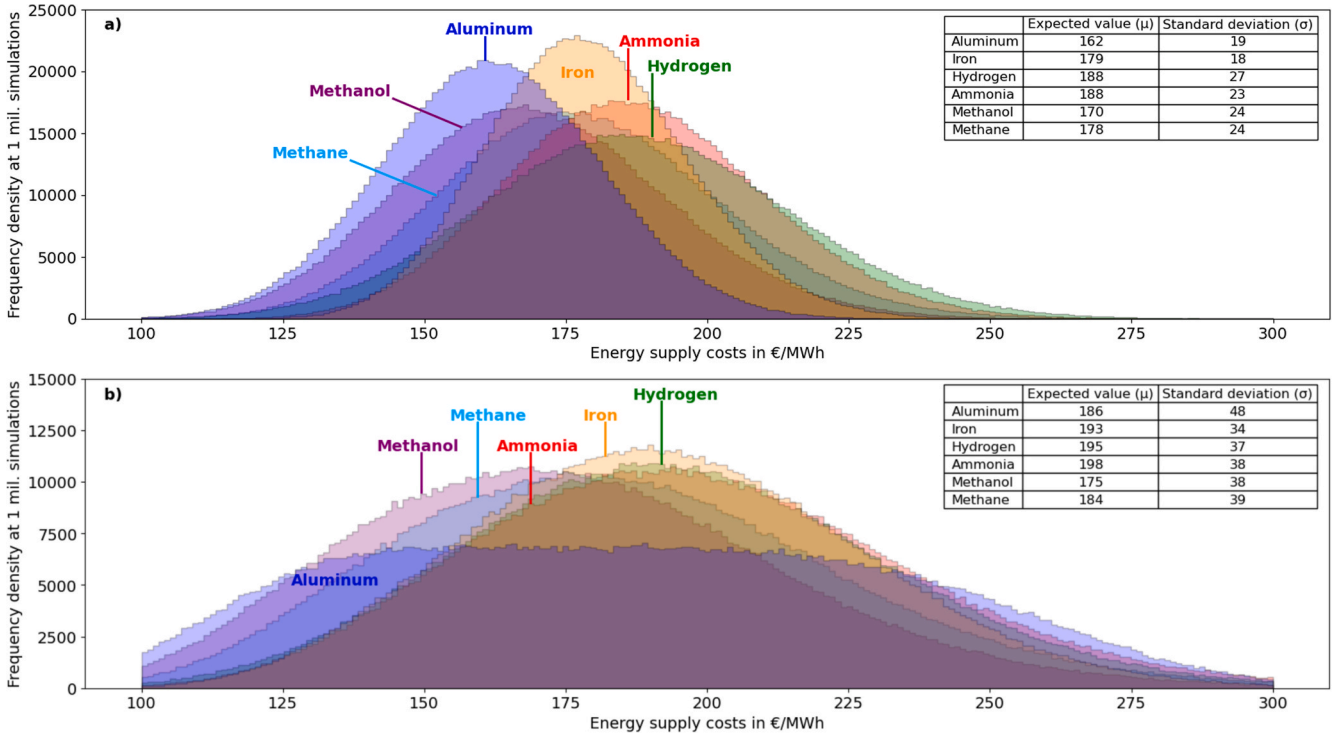

	Expected value (μ)	Standard deviation (σ)
Aluminum	162	19
Iron	179	18
Hydrogen	188	27
Ammonia	188	23
Methanol	170	24
Methane	178	24

	Expected value (μ)	Standard deviation (σ)
Aluminum	186	48
Iron	193	34
Hydrogen	195	37
Ammonia	198	38
Methanol	175	38
Methane	184	39

Fig. 7. Modified version of Fig. 5 using PSC instead of DAC for methanol and methane production.

Data availability

All used data is provided in the manuscript.

References

[1] Schmidt J, Gruber K, Klingler M, Klöckl C, Camargo LR, Regner P, et al. A new perspective on global renewable energy systems: why trade in energy carriers matters. Energ Environ Sci 2019;12:2022–9. https://doi.org/10.1039/C9EE00223E.
[2] IRENA, WTO, Enabling global trade in renewable hydrogen and derivative commodities, International Renewable Energy Agency and World Trade Organization, Abu Dhabi and Geneva, 2024.
[3] IEA, The Future of Hydrogen: Seizing today's opportunities, International Energy Agency, Paris, 2019. https://www.iea.org/reports/the-future-of-hydrogen.
[4] Hank C, Sternberg A, Köppel N, Holst M, Smolinka T, Schaadt A, et al. Energy efficiency and economic assessment of imported energy carriers based on renewable electricity. Sustain Energy Fuels 2020;4:2256–73. https://doi.org/10.1039/D0SE00067A.
[5] Johnston C, Ali Khan MH, Amal R, Daiyan R, MacGill I. Shipping the sunshine: an open-source model for costing renewable hydrogen transport from Australia. Int J Hydrogen Energy 2022;47:20362–77. https://doi.org/10.1016/j.ijhydene.2022.04.156.
[6] Moritz M, Schönfisch M, Schulte S. Estimating global production and supply costs for green hydrogen and hydrogen-based green energy commodities. Int J Hydrogen Energy 2023;48:9139–54. https://doi.org/10.1016/j.ijhydene.2022.12.046.
[7] Bergthorson JM. Recyclable metal fuels for clean and compact zero-carbon power. Prog. Energy Combust. Sci. 2018;68:169–96. https://doi.org/10.1016/j.pecs.2018.05.001.
[8] Halter F, Jeanjean S, Chauveau C, Berro Y, Balat-Pichelin M, Brilhac JF, et al. Recyclable metal fuels as future zero-carbon energy carrier. Appl Energy Combust Sci 2023;13:100100. https://doi.org/10.1016/j.jaecs.2022.100100.
[9] Kuhn C, Düll A, Rohlfs P, Tischer S, Börnhorst M, Deutschmann O. Iron as recyclable energy carrier: feasibility study and kinetic analysis of iron oxide reduction. Appl Energy Combust Sci 2022;12:100096. https://doi.org/10.1016/j.jaecs.2022.100096.
[10] Ning D, Shoshin Y, van Stiphout M, van Oijen J, Finotello G, de Goey P. Temperature and phase transitions of laser-ignited single iron particle. Combust Flame 2022;236:111801. https://doi.org/10.1016/j.combustflame.2021.111801.
[11] Wiinikka H, Vikström T, Wennebro J, Toth P, Sepman A. Pulverized sponge iron, a zero-carbon and clean substitute for fossil coal in energy applications. Energy Fuels 2018;32:9982–9. https://doi.org/10.1021/acs.energyfuels.8b02270.
[12] Chen R, Thijs LC, Hansen BB, Lin W, Wu H, Glarborg P, et al. Combustion of micron-sized iron particles in a drop tube reactor. Fuel 2025;383:133814. https://doi.org/10.1016/j.fuel.2024.133814.
[13] Nguyen B-D, Braig D, Scholtissek A, Ning D, Li T, Dreizler A, et al. Ignition and kinetic-limited oxidation analysis of single iron microparticles in hot laminar flows. Fuel 2024;371:131866. https://doi.org/10.1016/j.fuel.2024.131866.
[14] Julien P, Bergthorson JM. Enabling the metal fuel economy: green recycling of metal fuels. Sustain Energy Fuels 2017;1:615–25. https://doi.org/10.1039/C7SE00004A.
[15] Dirven L, Deen NG, Golombok M. Dense energy carrier assessment of four combustible metal powders. Sustain Energy Technol Assess 2018;30:52–8. https://doi.org/10.1016/j.seta.2018.09.003.
[16] Stevens NC, Prasidha W, Deen NG, Meeuwsen L, Baigmohammadi M, Shoshin Y, et al. Cyclic reduction of combusted iron powder: a study on the material properties and conversion reaction in the iron fuel cycle. Powder Technol 2024;441:119786. https://doi.org/10.1016/j.powtec.2024.119786.
[17] Wronski T, Sciacovelli A. Analysis of the potential of four reactive metals as zero-carbon energy carriers for energy storage and conversion. J Storage Mater 2024;100:113514. https://doi.org/10.1016/j.est.2024.113514.
[18] Barelli L, Baumann M, Bidini G, Ottaviano PA, Schneider RV, Passerini S, et al. Reactive metals as energy storage and carrier media: use of aluminum for power generation in fuel cell-based power plants. Energ. Technol. 2020;8:2000233. https://doi.org/10.1002/ente.202000233.
[19] Debiagi P, Rocha RC, Scholtissek A, Janicka J, Hasse C. Iron as a sustainable chemical carrier of renewable energy: analysis of opportunities and challenges for retrofitting coal-fired power plants. Renew Sustain Energy Rev 2022;165:112579. https://doi.org/10.1016/j.rser.2022.112579.
[20] Janicka J, Debiagi P, Scholtissek A, Dreizler A, Epple B, Pawellek R, et al. The potential of retrofitting existing coal power plants: a case study for operation with green iron. Appl Energy 2023;339:120950. https://doi.org/10.1016/j.apenergy.2023.120950.
[21] Kikkinides ES, Georgiadis MC, Stubos AK. Dynamic modelling and optimization of hydrogen storage in metal hydride beds. Energy 2006;31:2428–46. https://doi.org/10.1016/j.energy.2005.10.036.
[22] Lototskyy MV, Tolj I, Davids MW, Klochko YV, Parsons A, Swanepoel D, et al. Metal hydride hydrogen storage and supply systems for electric forklift with low-temperature proton exchange membrane fuel cell power module. Int J Hydrogen Energy 2016;41:13831–42. https://doi.org/10.1016/j.ijhydene.2016.01.148.

[23] Drawer C, Lange J, Kaltschmitt M. Metal hydrides for hydrogen storage – identification and evaluation of stationary and transportation applications. J Storage Mater 2024;77:109988. https://doi.org/10.1016/j.est.2023.109988.
[24] Ersoy H, Baumann M, Barelli L, Ottaviano A, Trombetti L, Weil M, et al. Hybrid energy storage and hydrogen supply based on aluminum - a multiservice case for electric mobility and energy storage services. Adv Mater Technol 2022;7:2101400. https://doi.org/10.1002/admt.202101400.
[25] Boudreau P, Johnson M, Bergthorson JM. Techno-economic assessment of aluminum as a clean energy carrier to decarbonize remote industries. Energy Adv 2024;3:1919–31. https://doi.org/10.1039/D4YA00151F.
[26] J. Neumann, R.C. Da Rocha, P. Debiagi, A. Scholtissek, F. Dammel, P. Stephan, C. Hasse, Techno-economic assessment of long-distance supply chains of energy carriers: comparing hydrogen and iron for carbon-free electricity generation, 2023. doi: 10.1016/j.jaecs.2023.100128.
[27] Genge L, Scheller F, Müsgens F. Supply costs of green chemical energy carriers at the European border: a meta-analysis. Int J Hydrogen Energy 2023;48:38766–81. https://doi.org/10.1016/j.ijhydene.2023.06.180.
[28] C. Hank, M. Holst, C. Thelen, C. Kost, S. Längle, A. Schaadt, T. Smolinka, Power-to-X Country Analyses, (2023). https://www.ise.fraunhofer.de/en/publications/studies/power-to-x-country-analyses.html (accessed March 5, 2024).
[29] Hampp J, Düren M, Brown T. Import options for chemical energy carriers from renewable sources to Germany. PLoS One 2022;18(2):E0262340. https://doi.org/10.1371/journal.
[30] Hessels CJM, Lelivelt DWJ, Stevens NC, Tang Y, Deen NG, Finotello G. Minimum fluidization velocity and reduction behavior of combusted iron powder in a fluidized bed. Fuel 2023;342:127710. https://doi.org/10.1016/j.fuel.2023.127710.
[31] finanzen.net, Eurokurs (EUR - USD) - Historische Kurse, (2024). https://www.finanzen.net/devisen/eurokurs#historisch.
[32] de Kwant J, Hekkenberg R, Souflis-Rigas A, Kana AA. Exploring the potential of iron powder as fuel on the design and performance of container ships. Int. Shipbuild. Prog. 2023;70:3–28. https://doi.org/10.3233/ISP-220012.
[33] Beswick RR, Oliveira AM, Yan Y. Does the green hydrogen economy have a water problem? ACS Energy Lett 2021;6:3167–9. https://doi.org/10.1021/acsenergylett.1c01375.
[34] Trowell KA, Goroshin S, Frost DL, Bergthorson JM. Aluminum and its role as a recyclable, sustainable carrier of renewable energy. Appl Energy 2020;275:115112. https://doi.org/10.1016/j.apenergy.2020.115112.
[35] acatech, BDI, A Meta-Analysis towards a German-Australian SupplyChain for Renewable Hydrogen: Working Paper HySupply, 2021. https://www.acatech.de/wp-content/uploads/2020/11/HySupply_WorkingPaper_Meta-Analysis.pdf.
[36] C. Kleinschmitt, J. Fragoso García, K. Franke, D. Teza, L. Seidel, A. Ebner, M. Baier, Weltweite Potenziale erneuerbarer Energien, HYPAT Working Paper 03/2022 (2022). https://doi.org/10.24406/publica-177 (accessed February 28, 2024).
[37] Schmidt O, Melchior S, Hawkes A, Staffell I. Projecting the future levelized cost of electricity storage technologies. Joule 2019;3:81–100. https://doi.org/10.1016/j.joule.2018.12.008.
[38] Levelized Cost of Energy+, Https://Www.Lazard.Com (2024). https://www.lazard.com/research-insights/levelized-cost-of-energyplus/ (accessed November 29, 2024).
[39] Realmonte G, Drouet L, Gambhir A, Glynn J, Hawkes A, Köberle AC, et al. An inter-model assessment of the role of direct air capture in deep mitigation pathways. Nat. Commun. 2019;10:3277. https://doi.org/10.1038/s41467-019-10842-5.
[40] Jensen EH, Andreasen A, Jørsboe JK, Andersen MP, Hostrup M, Elmegaard B, et al. Electrification of amine-based CO_2 capture utilizing heat pumps. Carbon Capture Sci Technol 2024;10:100154. https://doi.org/10.1016/j.ccst.2023.100154.
[41] Vogl V, Åhman M, Nilsson LJ. Assessment of hydrogen direct reduction for fossil-free steelmaking. J Clean Prod 2018;203:736–45. https://doi.org/10.1016/j.jclepro.2018.08.279.
[42] Bhaskar A, Abhishek R, Assadi M, Somehesaraei HN. Decarbonizing primary steel production: techno-economic assessment of a hydrogen based green steel production plant in Norway. J Clean Prod 2022;350:131339. https://doi.org/10.1016/j.jclepro.2022.131339.
[43] Brown T, Hampp J. Ultra-long-duration energy storage anywhere: methanol with carbon cycling. Joule 2023;7:2414–20. https://doi.org/10.1016/j.joule.2023.10.001.
[44] Runge P, Sölch C, Albert J, Wasserscheid P, Zöttl G, Grimm V. Economic comparison of electric fuels produced at excellent locations for renewable energies: a scenario for 2035. SSRN Electron J 2020. https://doi.org/10.2139/ssrn.3623514.
[45] Mohan A, Cheng F, Luo H, Greig C, Larson E, Jenkins JD. Direct air capture integration with low-carbon heat: process engineering and power system analysis. Energ. Conver. Manage. 2024;322:119136. https://doi.org/10.1016/j.enconman.2024.119136.
[46] Isogai H, Nakagaki T. Power-to-heat amine-based post-combustion CO_2 capture system with solvent storage utilizing fluctuating electricity prices. Appl Energy 2024;368:123519. https://doi.org/10.1016/j.apenergy.2024.123519.
[47] Alabdulkarem A, Hwang Y, Radermacher R. Multi-functional heat pumps integration in power plants for CO_2 capture and sequestration. Appl Energy 2015;147:258–68. https://doi.org/10.1016/j.apenergy.2015.03.003.
[48] Elsheikh H, Eveloy V. Renewable hydrogen based direct iron ore reduction and steel making with grid assistance. Energ. Conver. Manage. 2023;297:117544. https://doi.org/10.1016/j.enconman.2023.117544.
[49] Hybrit Development AB, Hydrogen Storage, (n.d.). https://www.hybritdevelopment.se/en/a-fossil-free-development/hydrogen-storage/ (accessed March 10, 2024).
[50] Ratvik AP, Mollaabbasi R, Alamdari H. Aluminium production process: from Hall–Héroult to modern smelters. ChemTexts 2022;8:10. https://doi.org/10.1007/s40828-022-00162-5.
[51] Lerede D, Bustreo C, Gracceva F, Saccone M, Savoldi L. Techno-economic and environmental characterization of industrial technologies for transparent bottom-up energy modeling. Renew Sustain Energy Rev 2021;140:110742. https://doi.org/10.1016/j.rser.2021.110742.
[52] Smith R. Chemical Process Design and Integration. 2nd ed. Chichester, West Sussex, United Kingdom: Wiley; 2016.
[53] Schuler J, Ardone A, Fichtner W. A review of shipping cost projections for hydrogen-based energy carriers. Int J Hydrogen Energy 2024;49:1497–508. https://doi.org/10.1016/j.ijhydene.2023.10.004.
[54] DNV, Securing Green Hydrogen for the German Power Sector, 2024. https://www.stiftung-klima.de/app/uploads/2024/10/DNV-Securing-Green-Hydrogen-for-the-German-Power-Sector_final-report.pdf.
[55] Akman M, Turan Bİ, Taşdemir A, Söğüt MZ. Alternative fuels for enhanced ship energy efficiency: a conceptual design study of a handymax bulk carrier. Int J Hydrogen Energy 2024. https://doi.org/10.1016/j.ijhydene.2024.11.069.
[56] Song S, Lin H, Sherman P, Yang X, Nielsen CP, Chen X, et al. Production of hydrogen from offshore wind in China and cost-competitive supply to Japan. Nat. Commun. 2021;12:6953. https://doi.org/10.1038/s41467-021-27214-7.
[57] Lopez G, Galimova T, Fasihi M, Bogdanov D, Breyer C. Towards defossilised steel: supply chain options for a green European steel industry. Energy 2023;273:127236. https://doi.org/10.1016/j.energy.2023.127236.
[58] Egerer J, Grimm V, Niazmand K, Runge P. The economics of global green ammonia trade – "shipping Australian wind and sunshine to Germany". Appl Energy 2023;334:120662. https://doi.org/10.1016/j.apenergy.2023.120662.
[59] Danish Energy Agency, Technology Catalogue for Carbon Capture, Transport and Storage, (2021). https://ens.dk/en/our-services/projections-and-models/technology-data/technology-data-carbon-capture-transport-and (accessed March 5, 2024).
[60] Danish Energy Agency, Technology Data for Renewable Fuels: Version 10, 08/2023, 2023. https://ens.dk/en/our-services/projections-and-models/technology-data/technology-data-renewable-fuels.
[61] Al-Breiki M, Bicer Y. Technical assessment of liquefied natural gas, ammonia and methanol for overseas energy transport based on energy and exergy analyses. Int J Hydrogen Energy 2020;45:34927–37. https://doi.org/10.1016/j.ijhydene.2020.04.181.
[62] Metalot, Vision document Iron Power - The potential of Iron Power technology in the energy transition, 2024. https://www.metalot.nl/en/news/2024-vision-document-iron-power/ (accessed August 7, 2024).
[63] Neumann J, Fradet Q, Scholtissek A, Dammel F, Riedel U, Dreizler A, et al. Thermodynamic assessment of an iron-based circular energy economy for carbon-free power supply. Appl Energy 2024;368:123476. https://doi.org/10.1016/j.apenergy.2024.123476.
[64] USGS National Minerals Information Center, Mineral commodity summaries 2023, USGS Publications Warehouse, 2023. https://doi.org/10.3133/mcs2023.
[65] Statista, Global aluminum and aluminum alloy trade 2021, Statista (2023). https://www.statista.com/statistics/491244/global-import-export-unwrought-aluminum-alloy-timeline/ (accessed March 1, 2024).
[66] International Aluminium Institute, Primary Aluminium Production, (2024). https://international-aluminium.org/statistics/primary-aluminium-production/ (accessed March 1, 2024).
[67] Raabe D. The materials science behind sustainable metals and alloys. Chem Rev 2023. https://doi.org/10.1021/acs.chemrev.2c00799.
[68] RioTinto, Rio Tinto to install carbon free aluminium smelting cells using first ELYSIS technology licence, Press Release (2024). https://www.riotinto.com/en/news/releases/2024/rio-tinto-to-install-carbon-free-aluminium-smelting-cells-using-first-elysistm-technology-licence (accessed May 12, 2025).
[69] RUSAL, RUSAL Conducts First-Ever Preheating and Start-Up of Aluminium Reduction Cell Using Inert Anodes, Press Release (2024). https://www.rusal.ru/en/press-center/press-releases/rusal-conducts-first-ever-preheating-and-start-up-of-aluminium-reduction-cell-using-inert-anodes/ (accessed May 12, 2025).
[70] Bai W, Qiao Y, Wang C, Li H, Zhang X, Zhang C, et al. Comprehensive assessments of a novel aluminum-fueled energy storage system. Energ. Conver. Manage. 2022;266:115615. https://doi.org/10.1016/j.enconman.2022.115615.
[71] Farmani A, Eskandari Manjili F. Modelling and assessment of hydrogen combined cycle power plant using aluminum-water reaction as renewable fuel. Int J Hydrogen Energy 2024;50:276–91. https://doi.org/10.1016/j.ijhydene.2023.08.239.
[72] Gorobez J, Maack B, Nilius N. Growth of self-passivating oxide layers on aluminum—pressure and temperature dependence. Physica Status Solidi (b) 2021;258:2000559. https://doi.org/10.1002/pssb.202000559.
[73] Nutrien Ltd., 2023 Fact Book, (2023). https://nutrien-prod-asset.s3.us-east-2.amazonaws.com/s3fs-public/uploads/2023-11/Nutrien_2023Fact%20Book_Update_112723.pdf (accessed March 1, 2024).
[74] Salmon N, Bañares-Alcántara R. Green ammonia as a spatial energy vector: a review. Sustain Energy Fuels 2021;5:2814–39. https://doi.org/10.1039/D1SE00345C.
[75] Gubbi S, Cole R, Emerson B, Noble D, Steele R, Sun W, et al. Air quality implications of using ammonia as a renewable fuel: how low can NOx emissions go? ACS Energy Lett 2023;8:4421–6. https://doi.org/10.1021/acsenergylett.3c01256.
[76] Bertagni MB, Socolow RH, Martirez JMP, Carter EA, Greig C, Ju Y, et al. Minimizing the impacts of the ammonia economy on the nitrogen cycle and

climate. Proc Natl Acad Sci 2023;120:e2311728120. https://doi.org/10.1073/pnas.2311728120.
[77] Capurso T, Stefanizzi M, Torresi M, Camporeale SM. Perspective of the role of hydrogen in the 21st century energy transition. Energ. Conver. Manage. 2022;251:114898. https://doi.org/10.1016/j.enconman.2021.114898.
[78] Hydrogen Council, McKinsey & Company, Hydrogen Insights 2023, (2023). https://hydrogencouncil.com/en/hydrogen-insights-2023/ (accessed March 1, 2024).
[79] International Energy Agency, Global Hydrogen Review 2023, (2023). https://iea.blob.core.windows.net/assets/ecdfc3bb-d212-4a4c-9ff7-6ce5b1e19cef/GlobalHydrogenReview2023.pdf (accessed March 1, 2024).
[80] IRENA, Global Hydrogen Trade to Meet the 1.5°C Climate Goal: Part II - Technology review of hydrogen carriers, International Renewable Energy Agency, Abu Dhabi, 2022. https://www.irena.org/publications/2022/Apr/Global-hydrogen-trade-Part-II.
[81] Ghafri SZA, Munro S, Cardella U, Funke T, Notardonato W, Trusler JPM, et al. Hydrogen liquefaction: a review of the fundamental physics, engineering practice and future opportunities. Energ Environ Sci 2022;15:2690–731. https://doi.org/10.1039/D2EE00099G.
[82] J. Fesmire, A. Swanger, Overview of the New LH2 Sphere at NASA Kennedy Space Center, (2021). https://www.energy.gov/eere/fuelcells/advances-liquid-hydrogen-storage-workshop (accessed March 1, 2024).
[83] Kawasaki Heavy Industries, Ltd., World's First Liquefied Hydrogen Carrier SUISO FRONTIER Launches Building an International Hydrogen Energy Supply Chain Aimed at Carbon-free Society, (2019). https://global.kawasaki.com/en/corp/newsroom/news/detail/?f=20191211_3487 (accessed March 1, 2024).
[84] Bergthorson JM, Goroshin S, Soo MJ, Julien P, Palecka J, Frost DL, et al. Direct combustion of recyclable metal fuels for zero-carbon heat and power. Appl Energy 2015;160:368–82. https://doi.org/10.1016/j.apenergy.2015.09.037.
[85] Kim J, Sovacool BK, Bazilian M, Griffiths S, Lee J, Yang M, et al. Decarbonizing the iron and steel industry: a systematic review of sociotechnical systems, technological innovations, and policy options. Energy Res Soc Sci 2022;89:102565. https://doi.org/10.1016/j.erss.2022.102565.
[86] Agora Industry, Wuppertal Institute for Climate, Environment and Energy, 15 Insights on the Global Steel Transformation, (2023). https://static.agora-energiewende.de/fileadmin/Projekte/2021/2021-06_IND_INT_GlobalSteel/A-EW_298_GlobalSteel_Insights_WEB.pdf (accessed March 1, 2024).
[87] Wang RR, Zhao YQ, Babich A, Senk D, Fan XY. Hydrogen direct reduction (H-DR) in steel industry—an overview of challenges and opportunities. J Clean Prod 2021;329:129797. https://doi.org/10.1016/j.jclepro.2021.129797.
[88] Ozkan M, Nayak SP, Ruiz AD, Jiang W. Current status and pillars of direct air capture technologies. iScience 2022;25. https://doi.org/10.1016/j.isci.2022.103990.